coatings

MDPI

Article

A Direct Laser Sintering Approach for the Electrophoretic Deposition Overlay of Yttria-Stabilized Zirconia on the Surface of a Thermal Barrier Coating System

Maryam A. Ali Bash *, Sami A. Ajeel, Ruqayah A. Abbas and Mohammed J. Kadhim

Department of Production Engineering and Metallurgy, University of Technology, Baghdad 19006, Iraq; sami.a.ajeel@uotechnology.edu.iq (S.A.A.); rukaia1990@yahoo.com (R.A.A.)
* Correspondence: maryam.a.alibash@uotechnology.edu.iq

Abstract: The laser sintering process and modification of yttria-stabilized zirconia (YSZ) coatings subjected to electrophoretic deposition (EPD) on YSZ air-plasma-sprayed (APS) thermal barrier coatings (TBCs) were investigated. A Ni-based superalloy was plasma-sprayed using yttria-stabilized zirconia (YSZ) to create a thermal barrier coating with a 400 µm thickness. The electrophoretic deposition (EPD) technique was used to deposit the nanopowder of YSZ on the surface of YSZ TBCs. In this study, a technology based on the direct sintering of a green EPD layer using a laser beam was employed. The best conditions for the deposition overlay of the YSZ coating using a DC current were obtained with an applied voltage of 40 V, deposition time of 5 min, and suspension concentration of 10 g/L. Iodine was added to the solutions as a stabilizing agent. To overcome the problems of high sintering temperatures, laser sintering was adopted as a new approach. The microstructures of all the specimens were studied using field emission scanning electron microscopy (FESEM) with energy-dispersive X-ray spectroscopy (EDS) analysis. Surface roughness was investigated using atomic force microscopy (AFM) analysis and the central line average (CLA). The direct laser sintering (DLS) process for the EPD overlay on the surface of the TBCs caused a reduction in surface roughness and porosity, and improvements in the microstructural and mechanical properties of the surface coatings were observed.

Keywords: thermal barrier coatings; YSZ; electrophoretic deposition; direct laser sintering

Citation: Ali Bash, M.A.; Ajeel, S.A.; Abbas, R.A.; Kadhim, M.J. A Direct Laser Sintering Approach for the Electrophoretic Deposition Overlay of Yttria-Stabilized Zirconia on the Surface of a Thermal Barrier Coating System. *Coatings* **2023**, *13*, 1695. https://doi.org/10.3390/coatings13101695

Academic Editors: Lei Guo, Jian He and Min Xie

Received: 31 August 2023
Revised: 21 September 2023
Accepted: 22 September 2023
Published: 27 September 2023

1. Introduction

Coating technology can help avoid or reduce structural degradation, corrosion, and wear, which leads to enhancement of durability, stability, and prolonged lifetime of the objects or surfaces to which it is applied [1,2]. Thermal-sprayed ceramic coatings are widely used in gas turbine and other heat engine components as thermal barrier coatings (TBCs) [3]. TBCs are used to protect metallic components from hot corrosion and oxidation and to reduce heat transmission [4]. YSZ is a material that is frequently employed in the design of sophisticated gas turbine engine systems [5]. Such coatings, which are based on ceramics with limited heat conductivity, provide thermal protection to actively cool metallic components. Due to its low cost, great efficiency, and ability to fabricate thick coatings, air-plasma-spraying APS is one of the most well-known and extensively utilized processes for TBC deposition [6]. In previous research, 8 wt.% Yttria-stabilized zirconia (8YSZ) showed a high thermal expansion coefficient, low thermal conductivity, and superior mechanical properties [7,8]. The porosity values of plasma-sprayed ceramic coatings are typically in the 3%–20% range [9]. High porosity may be desired for thermal barrier coatings, since porosity reduces the coating's thermal conductivity [10], while the performance aspects of these coatings, such as their corrosion resistance, toughness, and hardness, may be diminished with a high degree of porosity [11,12]. Several methods for improving these performance aspects have been proposed, including impregnation with polymers or ceramics, seal

sintering with liquid alloys, and post-laser irradiation. [13,14]. One unique technology that has the ability to eliminate porosity and produce a homogenous surface layer is laser surface treatment [15]. Laser remelting has been identified as a viable surface treatment for plasma-sprayed TBCs. It works by reducing the surface roughness of the ceramic coating, generating a fully dense layer, and sealing the open pores [16]. The laser treatment procedure involves heating, melting, and subsequent solidification, which results in surface sealing and a rise in TBC density. During laser treatment, cracks form, which is known to promote strain accommodation during thermal cycling. The effective factors for controlling crack networks are laser power, scanning speed, and track overlapping [17,18].

Homogeneous coatings created via electrophoretic deposition (EPD) can be deposited onto substrates with complex shapes and even porous structures [19]. When compared to alternative manufacturing techniques, electrophoretic deposition (EPD) produces homogeneous coatings at lower costs and faster speeds [20]. A post-EPD process is required to densify the coating and improve its mechanical properties, together with substrate adhesion. Typically, this post-EPD process is a heat treatment intended for the sintering of the coating; however, some precautions must be taken to avoid defects within the coating or at the interface with the substrate [21]. The sintering temperatures for YSZ are estimated to be 1400 °C or higher; moreover, shrinking the coatings through the sintering process may result in crack formation. Many approaches, such as fine-grained powders, microwave or irradiation treatment, and reaction bonding technology, can be employed to overcome the problems of high sintering temperatures [22,23]. The use of EPD coupled with the reaction bonding method can result in lower-than-usual sintering temperatures [4,24]. Furthermore, by controlling and selecting the correct sintering cycle, it is possible to obtain refined microstructures of the sintered bodies, as observed in spark plasma sintering, two-step sintering, and laser sintering [25]. Direct laser sintering is a novel technology in which the traditional heat source is replaced with a laser beam. Using this method, ceramic coatings with tiny grains and optimal general properties can be obtained. As a result, the investigation of new sintering processes is attracting attention from researchers, because it enables the optimization of density, grain sizes, and other critical ceramic properties [26].

To date, much literature has been published on the laser glazing of YSZ [27] and CYSZ [28] thermal barrier coatings; however, there is a dearth of research on the application of EPD overlay layers to TBCs. Therefore, this study will help to improve the TBC characteristics of YSZ coatings. The effect of direct laser sintering on the final microstructure of the EPD overlay is discussed, and it is shown that high-quality surface densification, a smooth surface, more reliable microhardness values, and uniform distribution of the elements of YSZ EPD coatings can be obtained through direct laser sintering.

2. Experimental Work

2.1. Materials and Coating Deposition Methods

The nickel-based superalloy Inconel 625 was used as the substrate material. Table 1 demonstrates the chemical composition of the substrate compared to the standard composition of the material. Air plasma spraying (APS) with the plasma gun type 3 MB, manufactured by Metco INC, Westbury, L.I.N.Y. (Westbury, NY, USA), was employed to obtain both a metallic bond coat and a ceramic top coat on the substrate surface in order to fabricate the TBC system. The bond and top coats were formed of Amdry 365-2 (Ni23Co17Cr12Al0.5Y) powder of a spherical shape and partially yttria-stabilized zirconia YSZ powder (ZrO_2 8 wt.% Y_2O_3, Metco 204 NS), respectively. The plasma spraying parameters are shown in Table 2. The electrophoretic deposition process (EPD) was carried out to deposit a layer on the TBC system using nano-sized YSZ powder (ZrO_2 5 mol% Y_2O_3) (NanoAmor, Houston, TX, USA), as in a previous study [10]. The EPD procedures were carried out in a steady colloidal solution of nano-YSZ powder in an organic solvent (ethanol) containing 1.0% acetic acid. In addition, iodine (I_2) at a 0.5 g/L concentration was used. To generate a stable colloidal solution of individually distributed YSZ particles, all suspensions were agitated mechanically for 24 h and then ultrasonically for 40 min to

break down the particle conglomerate. The parameters of (40 V, 5 min, 10 g/L YSZ) were utilized to create a uniform overlay layer. The equipment for the EPD process consisted of a power supply (DC model: Rayannik DC power supply 6005-D.), hot plate stirrer (DAIHAN Lab Tech/Model: LSM-1003), ultrasonic cleaning bath (Elmasonic P 30H ultrasonic bath, Singen am Hohentwiel, Germany), and balance with 4-digit presentation (AND GR-202 analytical balance, Tokyo, Japan) for weighing the powders used for deposition. The working electrode must have an electrically conductive surface to facilitate the EPD process on non-conductive substrates and for regular deposition. As a result, a thin layer of Pt was deposited onto the APS YSZ coatings using a DC sputtering coating system (model: DSR1).

Table 1. Chemical composition of the substrate Inconel 625.

Elements (wt.%)	Ni	Cr	Fe	Mo	Nb	Co	Mn	Ti	Al
Measured	62.03	22.06	2.85	8.43	3.48	0.04	0.14	0.33	0.24
Standard (ASTM)	Min 58	20–23	5	8–10	3.15–4.15	1	0.5	0.4	0.4

Table 2. Plasma spraying parameters for the bond and ceramic coatings used in this study.

Parameters	Bond Coat	Ceramic Coat
Current, Ampere	450	500
Primary gas	Ar	Ar
Pressure, psi	100	100
Flow rate, SCHF	85	85
Voltage, Volt	55	60
Secondary gas	H_2	H_2
Pressure, psi	50	50
Flow rate, SCHF	15	15
Spray distance, mm	120	100
Angle, %	90°	90°
Carrier	Ar	Ar
Flow rate, SCHF	40	50
Powder feed rate, g/min	40	80

2.2. Laser Sintering of EPD Overlay

The green EPD specimens were sintered and modified using a laser beam directly in one step. The laser remelting treatment was carried out using an Nd:YAG solid-state laser in the pulse-wave mode. The Nd:YAG laser-made Model PMT4297 was used in this study. It emits radiation at a single wavelength of 1064 nm. Laser beams were applied during the sintering of the EPD coating surface. Tables 3 and 4 show the laser process parameters used for laser sintering and the characteristics of the used Nd:YAG laser, respectively.

Table 3. Process parameters of the laser sintering process.

Parameters	Value
Average Power, (P)	55 W
Pulse frequency, (f)	60 Hz
Laser peak power, (Pp)	0.3 KW
Pulse energy, (PE)	0.91 j
Traverse speed, (V)	4 mm/s
Pulse duration (pulse length), (t)	3 ms
Beam diameter, (d)	1.6

Table 4. General characteristics of Nd: YAG laser used.

Characteristic	Value
Wavelength	1064 nm
Transverse mode	TEM00
Laser beam diameter	8 mm
Maximum power	500 W
Voltage	380 V, 3 phases, 50 Hz
Voltage stability	±5%
Minimum spot diameter	Approximately 400 μm
Operating mode	Pulse
Spectral width, W	Less than 3 nm
Wall plug efficiency	About 5%

2.3. Hot Corrosion Test

The coatings were ultrasonically cleaned with ethanol and dried before the hot corrosion testing. Subsequently, the Na_2SO_4—55% V_2O_5 (Merck, Sigma Aldrich, Darmstadt, Germany) mixture was used as corrosive salts. The salt mixture was placed on the surface of the coating with a concentration of 30 mg/cm^2, which uniformly spread at the center of the coating surface in order to avoid the edge effect. The samples were then heated in an electric furnace at 1000 °C in an air environment for 90 h. After that, they were kept inside the furnace chamber to cool to ambient temperature.

2.4. Characterization Procedure

The microstructure of the investigated coatings was examined using a field emission scanning electron microscope (FESEM: MIRA3-VP TESCAN, Czech Republic). Mercury Intrusion Porosimetry (MIP) thermo Finnigan, Instrument type: Pascal 140, was used to measure the pore size distribution of the samples. The X-ray diffraction (XRD: Rigaku, Tokyo, Japan) test was utilized to determine the phases presented in all the coated samples. The central line average (CLA) roughness was characterized using a roughness tester (Hommelwerke T8000 stylus profilometer, Villingen-Schwenningen, Germany) and the nanoroughness was investigated using atomic force microscopy (AFM:SPM AA3000, Angstrom advanced Inc., Stoughton, MA, USA) analysis. The microhardness value was determined using a digital micro-Vickers hardness tester TH714. The applied load for producing microscopic indentations was 0.5 kg for a duration of 15 sec. Weibull's distribution approach was performed to obtain microhardness reliability values. The elements present on the surface were identified with an energy dispersive spectroscope (EDS) attached to the FESEM.

3. Results and Discussion

3.1. Microstructure Evaluation

The air plasma sprayed coating's microstructure is extremely complicated and heterogeneous. Figure 1 shows typical FE-SEM micrographs of the upper surface view. They clearly demonstrated a rough appearance, a non-uniform and uneven distribution of open porosity, unmelted particles, semi-melted particles, and a network of cracks inside the splats. The existence of intrasplat cracks in the splat structure was attributed to residual process stresses. Pores can form between the splats for a number of causes, including trapped gas, insufficient filling of previously deposited particle holes, poor inter-splat interface contact, or insufficient melted particles to fill the surface irregularities. Using image J software ImageJ (version 1.47 for Windows, 64-bit, free software, National Institutes of Health, Bethesda, MD, USA), the percentage of open porosity was estimated to be around 14%. This general microstructure is due to the rapid solidification of the plasma-spraying process.

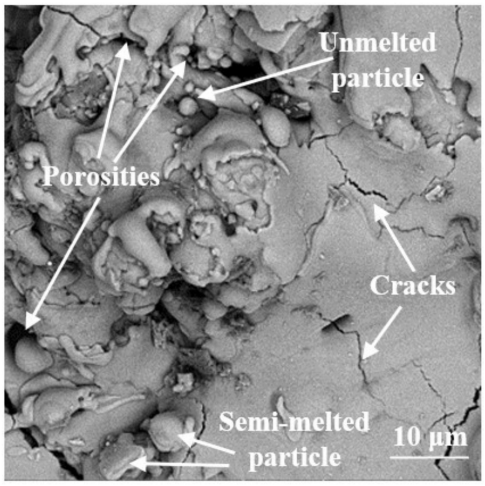

Figure 1. FE-SEM micrograph of the surface morphology of plasma sprayed coating.

Figure 2a depicts the cross-sectional microstructure of the components. The microstructure is revealed to be composed of a multilayer of metallic bond coat, YSZ ceramic topcoat, and a thin layer of thermally generated oxide (TGO) at the bond coat/ceramic interface. There are various vertical and horizontal cracks with porosity, which are typical APS process flaws. The element distribution in the plasma sprayed coating was shown by a typical EDS analysis in Figure 2b,c. As the main constituents of YSZ coatings, it is composed of Zr, Y, and O elements. The elements for the bond coat, are Ni, Co, Cr, Al, and Y.

The deposition rate of nano YSZ on the surface of plasma sprayed coating using the EPD process mostly depended on the EPD process parameters and suspension parameters. The best parameters resulted from the optimizing coating thickness of electrophoretic deposition overlay in [13] was utilized (40 V, 10 g/L, and 5 min). The surface morphology of the green EPD overlay on the APS TBCs is shown at low magnification in Figure 3a and high magnification in Figure 3b. One can observe the uniformity and homogeneity of the coating layer, as well as the formation of flat and smooth surfaces. MIP measurements in Figure 4 demonstrate the pore size distribution of both plasma sprayed coatings before applying the EPD overlay and after the green EPD overlay. The cumulative liquid mercury volume as a function of pressure is used to compute the pore size distribution. Mercury porosimetry Figure 4a shows that the majority of the pore volume lies in the macroporous size range of the pore diameter 5.5 to 137.7 µm. The pore size distribution after EPD overlay Figure 4b lies in the nanoporous size range of the pore diameter 12.21 to 9346.69 nm. This lack of pores was critical for preventing the inward diffusion of harmful substances such as CMAS and oxygen from the environment through the structure of the plasma-sprayed

coating beneath during service. Therefore, the probability of component failure due to oxidation or hot corrosion will be reduced.

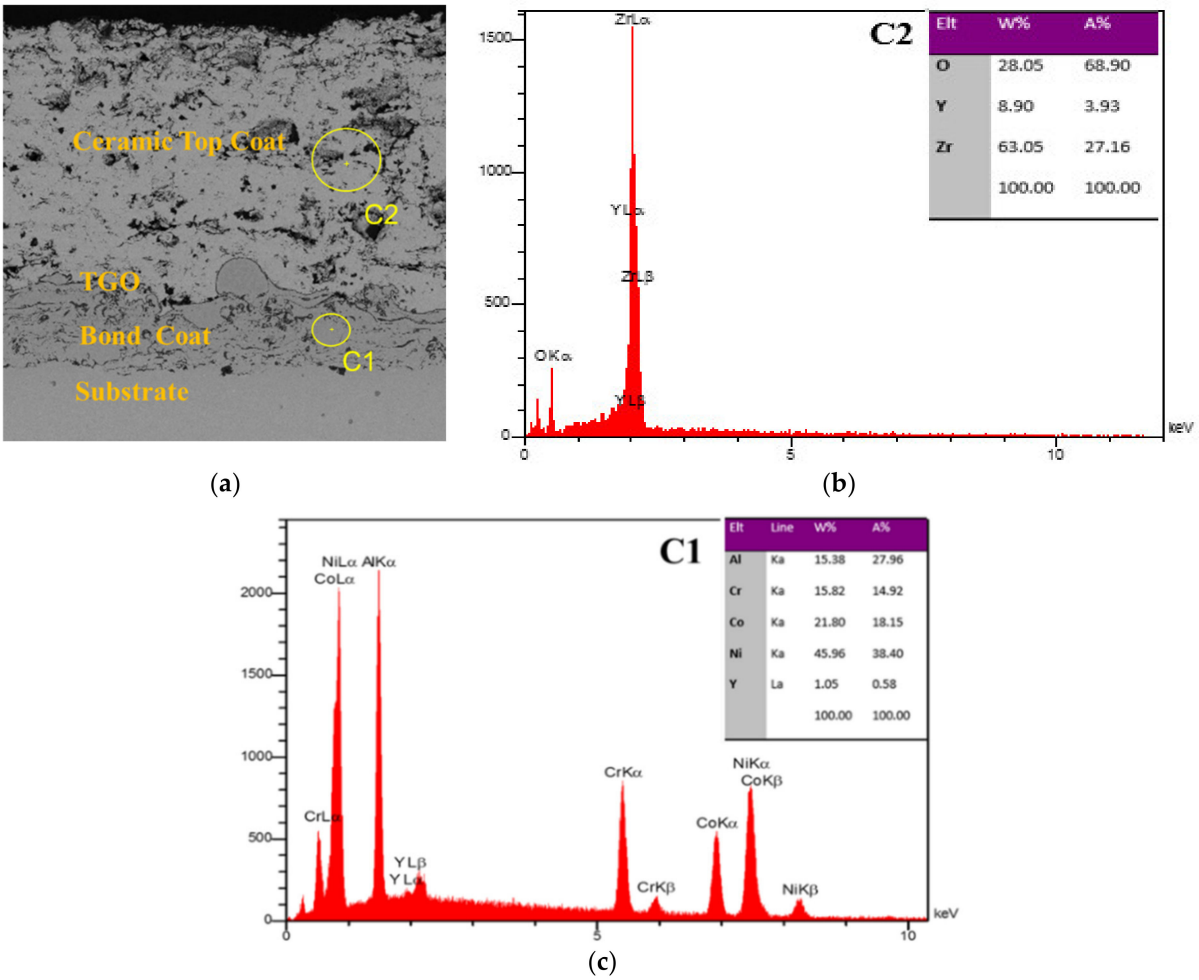

Figure 2. FE-SEM (**a**) and EDS analysis for the cross-section of plasma sprayed TBCs for ceramic top coat (**b**) and bond coat (**c**).

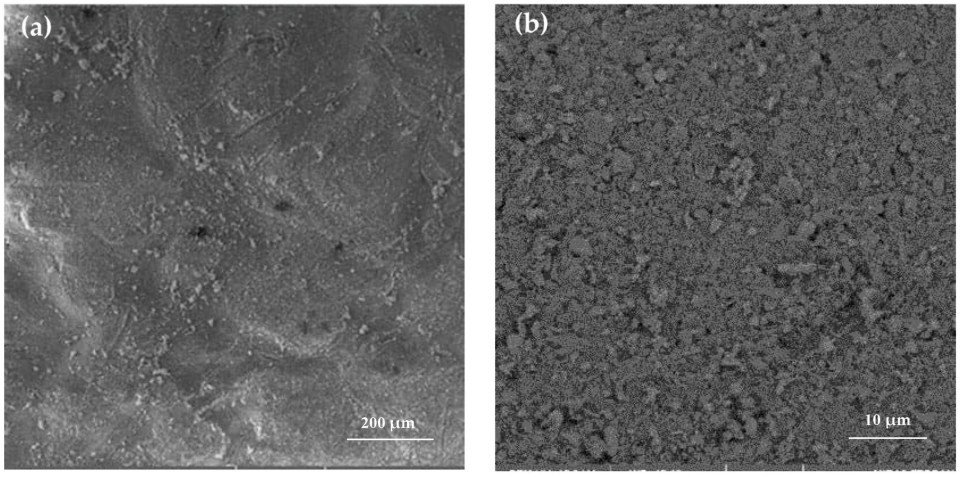

Figure 3. FE-SEM of the surface morphology of the EPD overlay on plasma-sprayed YSZ TBCs at (**a**) low magnification and (**b**) high magnification.

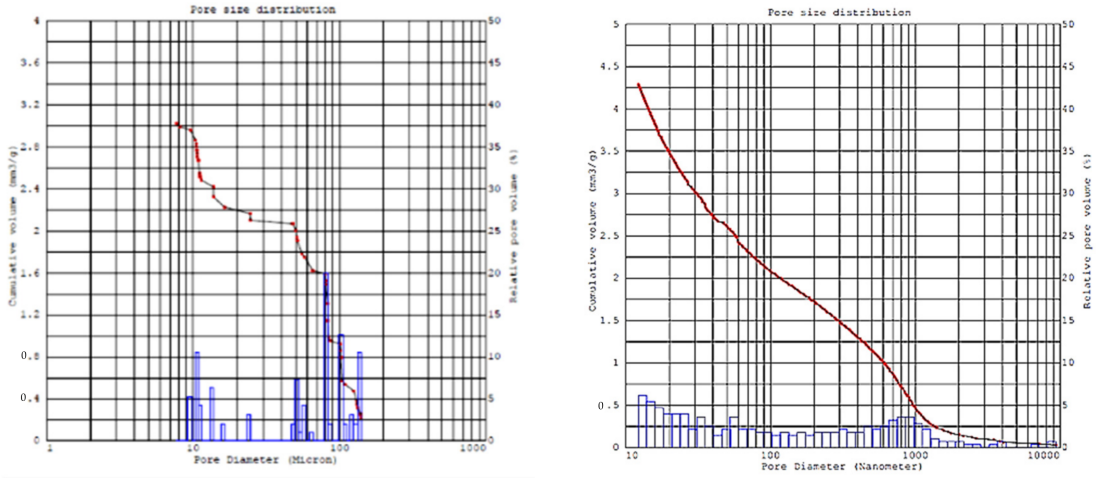

(a) **(b)**

Figure 4. Frequency and pore size distribution of (**a**) as-sprayed coating [9] (**b**) EPD overlay surface.

Figure 5a shows a cross-section of the YSZ nanocoatings, to which we applied a voltage of 40 V for 5 min and a concentration of 10 g/L. It can be observed that the EPD overlay thickness of the YSZ nanocoating is approximately 110 µm in Figure 5b. The coating maintained a dense, continuous, and crack-free morphology. The contact between the EPD overlay coating and the APS coating clearly provided good adherence. The quality of the green YSZ EPD overlay depended strongly on the stability of the suspension used. The use of iodine as a dispersant in suspension enhances the formation of free protons through the reaction between I_2 and the ethanol solvent. A sufficient amount of iodine was added to the suspension as a dispersant at a level of approximately 0.5 g/L to adjust the particles' surface charge in the YSZ EPD suspension, resulting in high zeta potential and mobility at 10 g/L concentration as in [13].

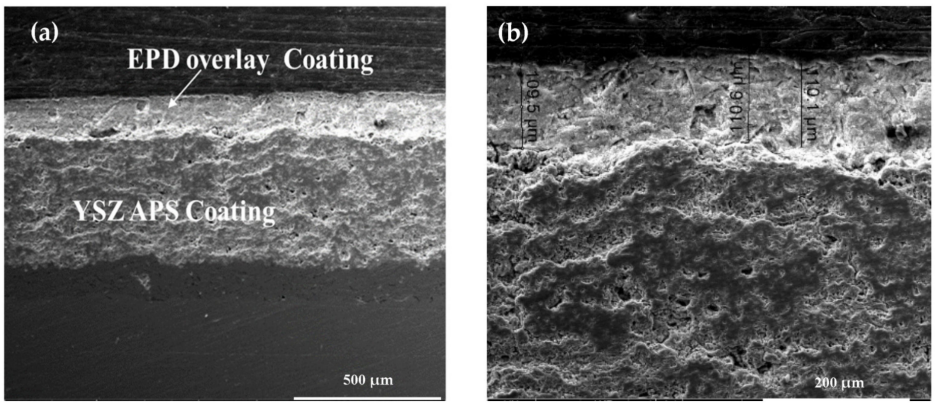

Figure 5. FE-SEM images of the cross-section of the EPD overlay on plasma-sprayed TBC surfaces at (**a**) low and (**b**) high magnification showing the homogeneity of the coating.

The green EPD overlay was dried at room temperature for 24 h before it was laser-sintered. Figure 6 demonstrates the surface top view of the direct-laser-sintered EPD overlay. An obvious change in the surface structure can be observed. At a low magnification, Figure 6a shows a smooth appearance and a network of segmented cracks distributed throughout the whole laser-treated surface. Grain refinement can be observed at a high magnification in Figure 6b. The cells are distributed in different sizes, which reflects the solidification mechanism occurring after laser treatment, associated with a high cooling rate [29]. The laser's interaction with the nonhomogeneous surface causes different temperature absorption areas, resulting in different solidification rates.

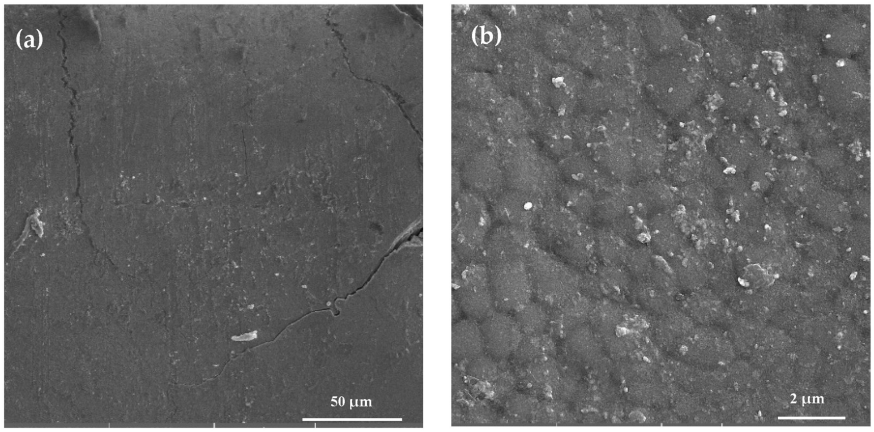

Figure 6. FE-SEM with (**a**) low and (**b**) higher magnification of the upper surface subjected to direct laser sintering, showing the small network of cracks and cells.

It can be concluded that it is possible to use the laser beam to directly sinter and modify the green EPD overlay in one step, instead of sintering the green layer using an electrical furnace followed by modification of the surface using a laser beam (two steps). Our selection of the appropriate laser parameters (power, scanning speed, and pulse length) resulted in continuous and consistent laser tracks. A power density of 150 W mm^{-2} and a specific energy of 8.593 J mm^{-2} are sufficient to produce densified and homogeneous ceramic coatings. Figure 7a demonstrates the consistent distribution of elements (Zr, O, and Y) in the surface layer, with the mapping shown in Figure 7b.

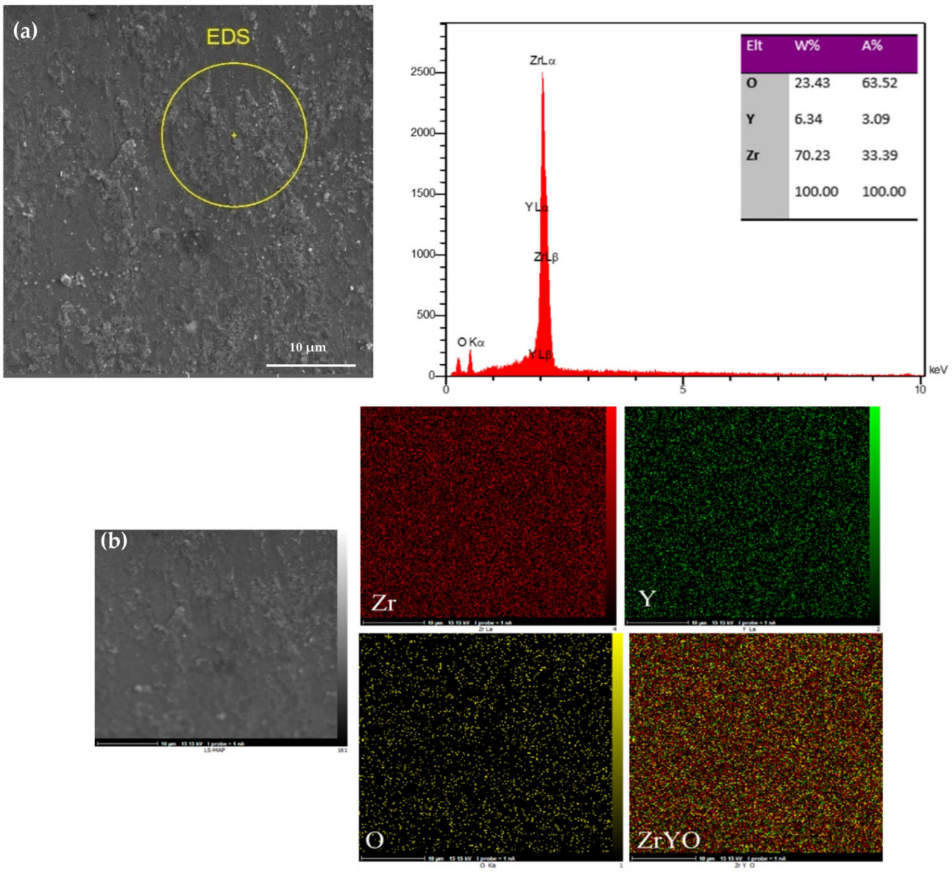

Figure 7. (**a**) EDS analysis with (**b**) mapping after the direct laser sintering process for the EPD overlay.

The cross-sectional FE-SEM micrograph of the green EPD overlay coating after laser sintering is illustrated in Figure 8. The laser irradiation beam produced a remelted overlay with a densified microstructure and a network of segmented cracks, which are perpendicular to the surface. The maximum depth of complete laser melting was measured from the FE-SEM images at approximately 41 µm.

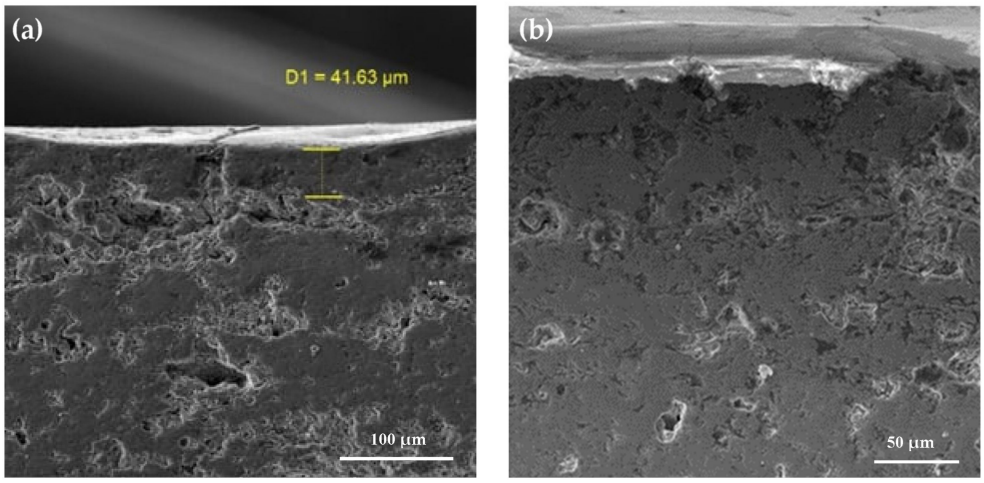

Figure 8. The cross-section of the densified green EPD overlay subjected to direct laser sintering, showing (**a**) the maximum depth of melting and (**b**) the general appearance.

The FE-SEM micrograph of the interface between the YSZ EPD overlay and the direct laser sintering region is presented in Figure 9, which shows the contrast. It can be revealed that the laser sintering track has a completely different microstructure than those of the EPD region when the heat input is sufficient for surface remelting. It can be concluded that the heat input of 13.75 J/mm was sufficient to sinter and modify the green EPD overlay.

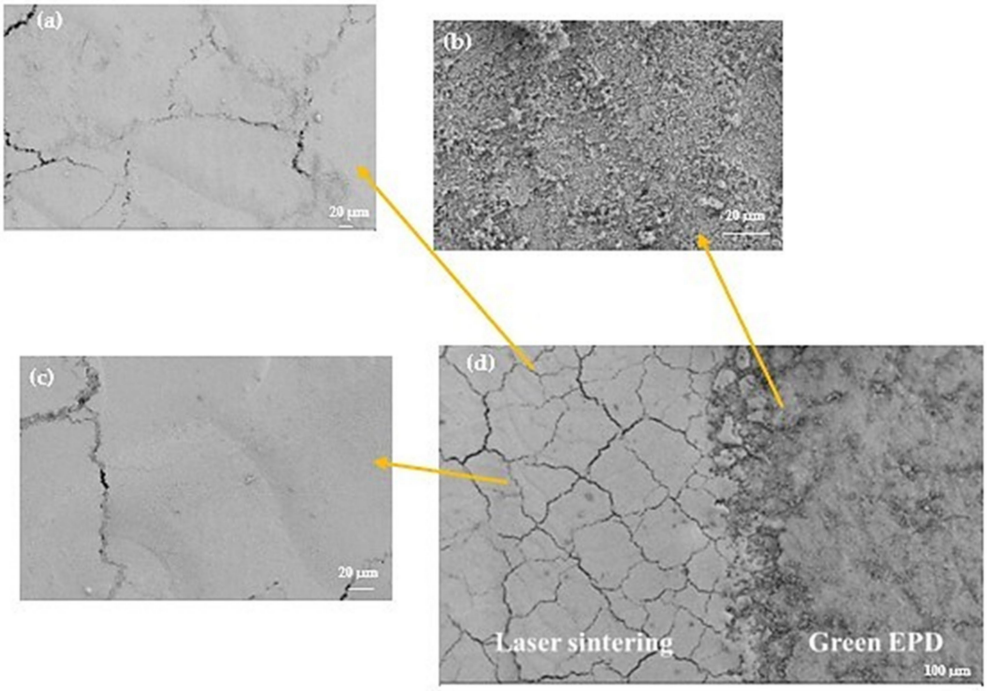

Figure 9. FE-SEM for the interface between the EPD overlay and the direct laser sintering region showing the surface modification (**a**,**c**), laser sintering region, (**b**) EPD overlay region, and (**d**) the contact between two regions.

Figure 10 shows the XRD pattern of the green YSZ overlay deposited via the EPD method. It demonstrates that the structure consists of transformable tetragonal (t) phases as a predominant phase, with a minimal monoclinic (m) phase, while the direct laser sintering process of the YSZ overlay deposited via EPD coating clearly shows the non-transformable (t′) tetragonal phase alone, as shown in Figure 10. Because the green EPD coating was formed at room temperature, no phase transformation occurred. However, the (t′) phase occurred due to diffusionless transformation as a result of fast cooling during the laser treatment. It is important to mention the absence of a monoclinic phase in the direct laser sintering of the coating. This concerns one of the enhancements in this work, as compared with the plasma-sprayed YSZ thermal barrier coatings shown in Figure 11. It can be observed that the coating consists of a non-transformable (t′) tetragonal phase, containing a minimal monoclinic (m) phase. Top coat oxide phase stability is an essential factor in optimizing TBC performance. This means that the presence of the (m) phase is likely to lead to subsequent transformations during the service of the coating layer, in contrast to the presence of the non-transformed (t′) phase, which increases the stability of the coating.

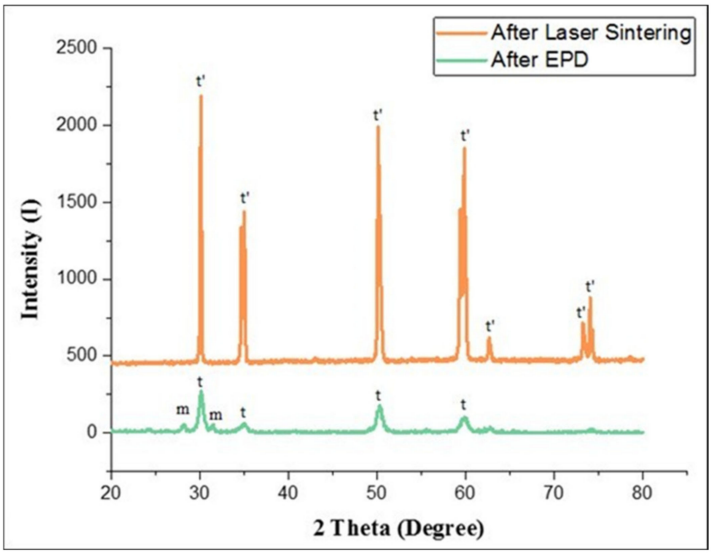

Figure 10. XRD pattern of YSZ overlay subjected to the EPD process and after the laser sintering of the overlay.

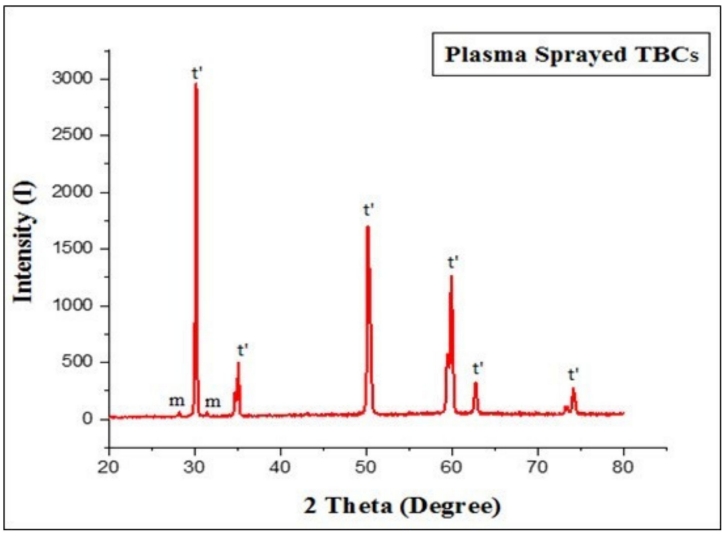

Figure 11. XRD pattern of plasma-sprayed YSZ thermal barrier coating.

In the microhardness measurements following direct laser sintering (DLS), as demonstrated in Figure 12 and Table A1 (Appendix A), there was significant variance in the hardness value of the same specimen, ranging between (957) and (1809) Hv. Due to the heterogeneous structure of the plasma-sprayed coating, which is composed of (melted, semi-melted, and non-melted) particles on the surface and, as a consequence, contains defects such as pores, with a network of cracks inside the splats [30], wide scattering from the mean value of the measured feature (microhardness) was observed. Hence, another approach was required to increase the reliability of the investigated property, and Weibull's distribution approach was applied [30]. The microhardness value for the plasma-sprayed YSZ thermal barrier coating was only 603 Hv. For more details, see [30]. In contrast, after the two methods of enhancement, namely, the EPD overlay and laser sintering process, there was an increase in the microhardness value to 1376 Hv. This higher microhardness after the laser sintering process was mostly due to the lack of porosity and fine grains in the remelted zone.

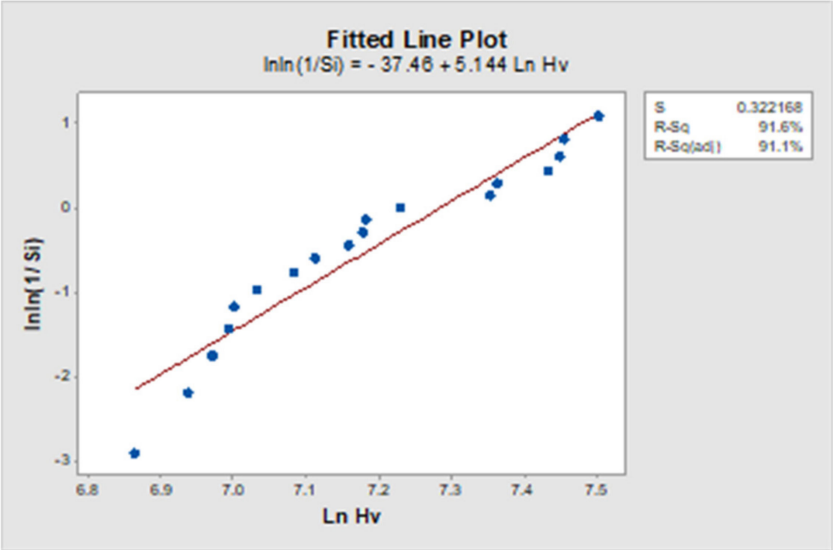

Figure 12. Weibull's distribution of microhardness values for laser-modified coatings treated with direct laser sintering (DLS).

3.2. Surface Roughness

The CLA roughness and nanoroughness measurements can be observed in Figures 13 and 14. One can clearly observe the decrease in the roughness values after the modification of the thermal barrier coating surfaces via EPD overlaying and the following laser sintering process.

The previously obtained initial Ra measurements of the surfaces of the as-sprayed coatings at a spray distance of 100 mm were around 8.6 µm [30]. It is possible to observe the roughness profile, and due to the heterogeneous microstructure generated from the plasma-spraying technique, featuring microcracks and partially molten particles, it is highly inconsistent and rough, while the surface roughness after the application of the EPD overlay was decreased to 5.36 µm, as compared with the coating subjected to plasma spraying alone. The fine particles were spread consistently, which increased the level of homogeneity and resulted in crack-free coatings. The nanoroughness value of the green EPD was (2.32) nm. These results were also confirmed through FE-SEM observation. All the roughness results are summarized in Table 5.

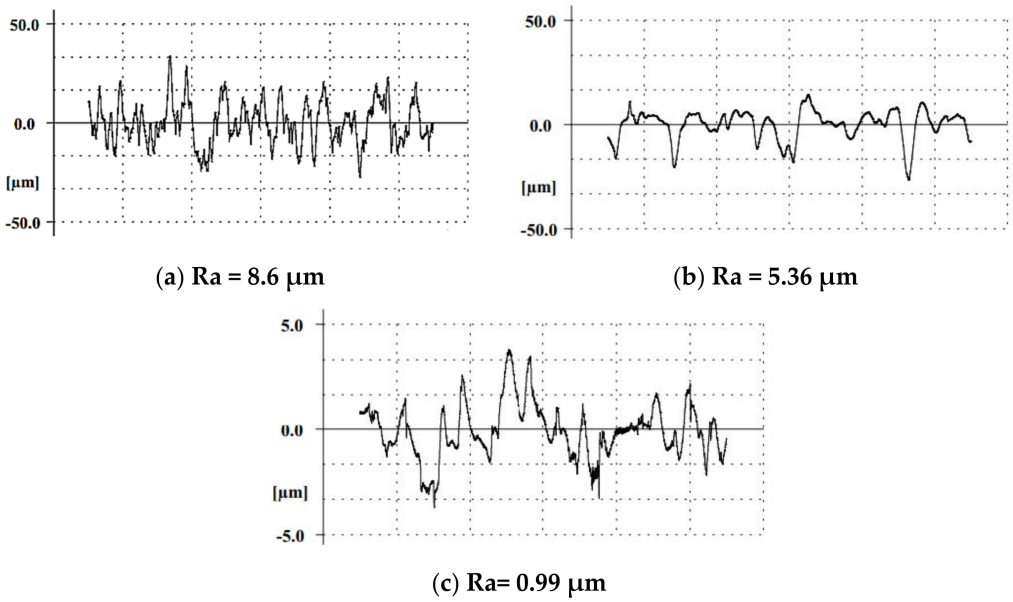

Figure 13. The microroughness profile of (**a**) specimens subjected to plasma spraying at a 100 mm spray distance, (**b**) EPD overlay, and (**c**) direct laser sintering.

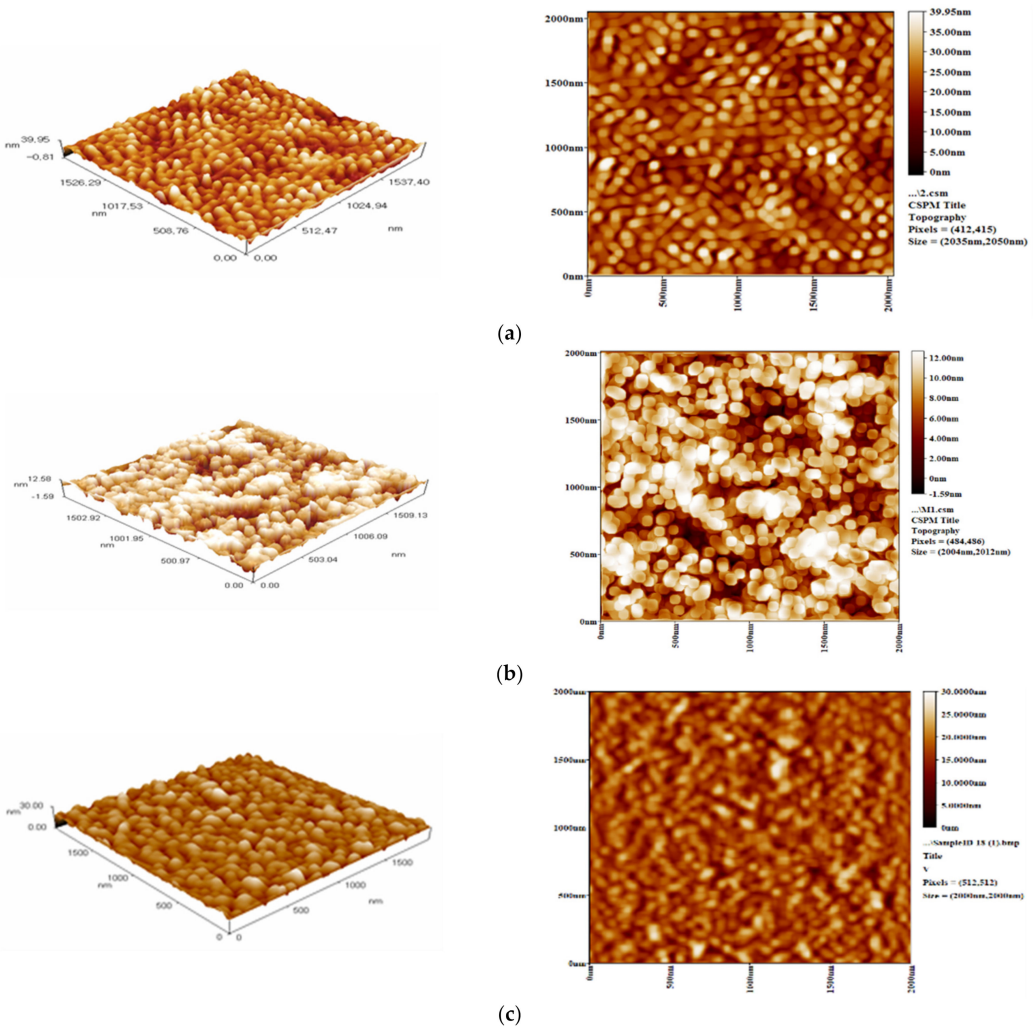

Figure 14. The two- and three-dimensional images from the AFM analysis of coatings for (**a**) specimens subjected to plasma spraying, (**b**) EPD overlay, (**c**) and direct laser sintering (LS).

Table 5. Average values of the CLA roughness and nanoroughness for all specimens.

No.	Specimens	Ra, µm	Ra, nm
1	Plasma coated	8.609	4.38
2	Green EPD	5.36	2.32
3	Direct laser sintering	0.99	2.48

Direct laser sintering is a promising technique for the densification of green EPD layers with a dispensed furnace sintering step. There are many benefits of this technique, including the possibility of obtaining a high-density surface and good microstructure. The improvement in the roughness behavior is typically attributed to the sufficient amount of energy applied to the full surface for the modification of the green EPD layer. The CLA roughness value decreased to 0.99 µm after the laser sintering process, while the AFM results showed that the roughness decreased to 2.48 nm. It can also be observed from the AFM analysis that the shadow effect was absent, which indicates a very low roughness value due to the lack of defects. The 3D images demonstrated clear changes in the microstructure after the laser sintering process and the homogenous distribution of the particles.

Surface modification with a laser irradiation beam is effective as a post-processing treatment and proved to be capable of reducing surface roughness. It can be concluded that it is possible to decrease surface roughness using an appropriate method of surface enhancement. Both the EPD overlay and laser treatment decrease roughness. This means that the performance of the thermal barrier coating can be greatly improved.

3.3. Hot Corrosion

The surface morphologies of the plasma-sprayed YSZ coating before and after modification with EPD overlay and direct laser sintering after 90 h of hot corrosion at 1000 °C are shown in Figure 15. The plasma-sprayed coating appeared to be almost completely covered with rod-like crystals, indicating the existence of chemical corrosion between the molten salts and the YSZ coating. Figure 15b,c shows the corrosion products of the plasma-sprayed coating at higher magnification. Many plate-shaped crystals stacked on top of each other, as well as a few cubic-shaped crystals, were observed. It is important to note that the corrosion products on the surfaces of the direct laser sintering of the EPD overlay sample are identical to those of the original plasma sprayed coatings due to the same formation procedure Figure 15d–f. The corrosion products of the remelting coating consist of certain extended rod-shaped crystals that are spread uniformly on the remelting coating's surface. However, the attack by corrosion salts (V_2O_5 + Na_2SO_4) was greater in the case of plasma-sprayed YSZ coating without surface modification than in the case of direct laser sintering of the EPD overlay. This was due to the presence of open porosity on the plasma coating's surface, which acts as a salt concentration pocket. As a result, the molten salts can easily penetrate the coating structure via the flaws. Furthermore, the specific surface area for the corrosion reaction was high due to the morphology of the surface of the plasma sprayed coating (extremely rough surface) Figure 15a compared to the smooth surface after laser treatment Figure 15d.

After laser treatment, rod-like crystals were reduced and corrosion resistance was improved as compared to plasma-sprayed coating. This is mainly due to the removal of pores and cracks by the use of nano-sized YSZ powder deposited using the EPD method and subsequent laser modification. This resulted in sealing the surface and the penetration pathways of molten salts into the plasma sprayed covering being reduced. The formation of rod-like crystals (YVO_4) can be attributed to the reaction of the stabilizer Y_2O_3 in zirconia-based TBCs with corrosion salts. This is confirmed by SEM micrograph and EDS analysis in Figures 16 and 17. According to EDS analysis from point A in (Figures 16 and 17), these rod-like crystals contain Y, V, and O, whereas the matrix (region B) contains Zr, Y, V, and O.

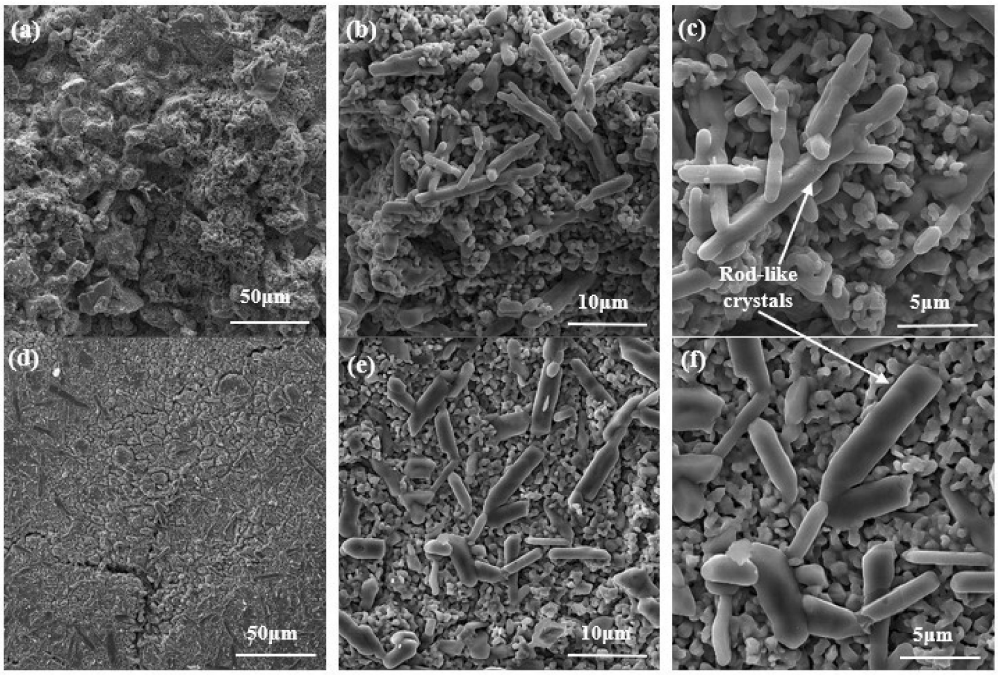

Figure 15. FE-SEM surface morphology of the plasma-sprayed coating after the hot corrosion test at 1000 °C for 90 h. (**a**) Lower magnification; (**b**,**c**) higher magnification. (**d**) After direct laser sintering of EPD overlay on the surface of plasma sprayed coating. (**e**,**f**) Higher magnification of (**d**).

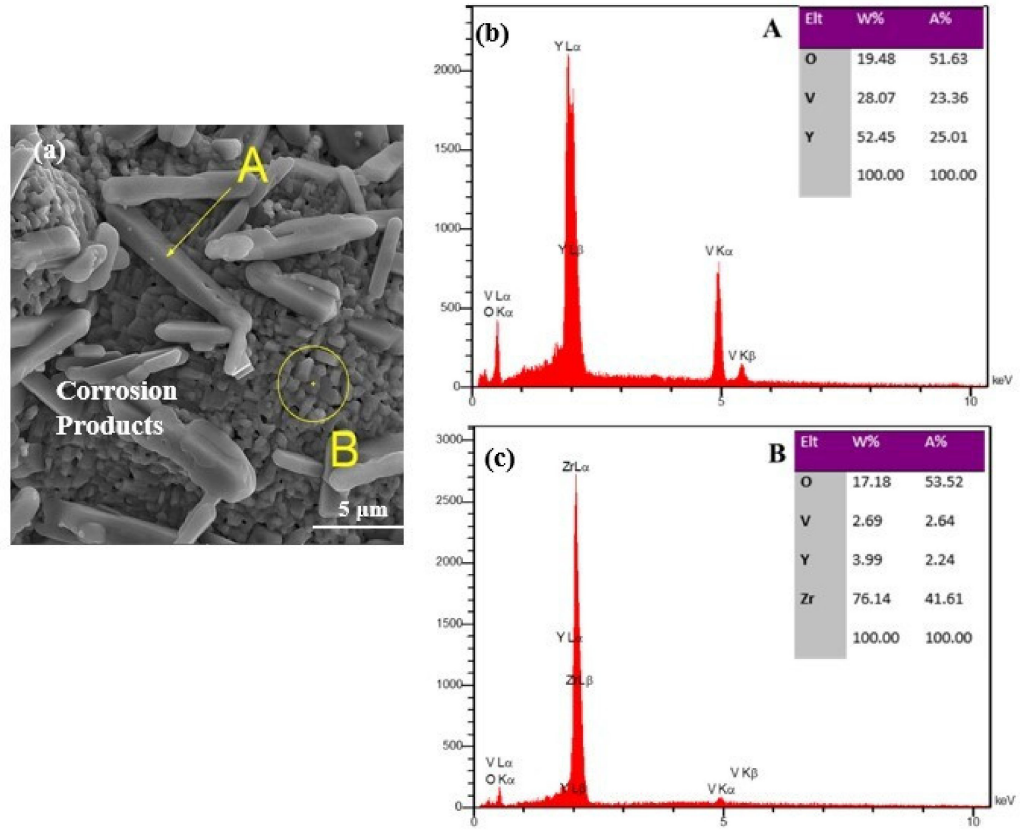

Figure 16. FE-SEM micrographs and EDS analysis of the plasma sprayed coating after hot corrosion, (**a**) the surface of the coating, (**b**) EDS of point A, (**c**) EDS of area B.

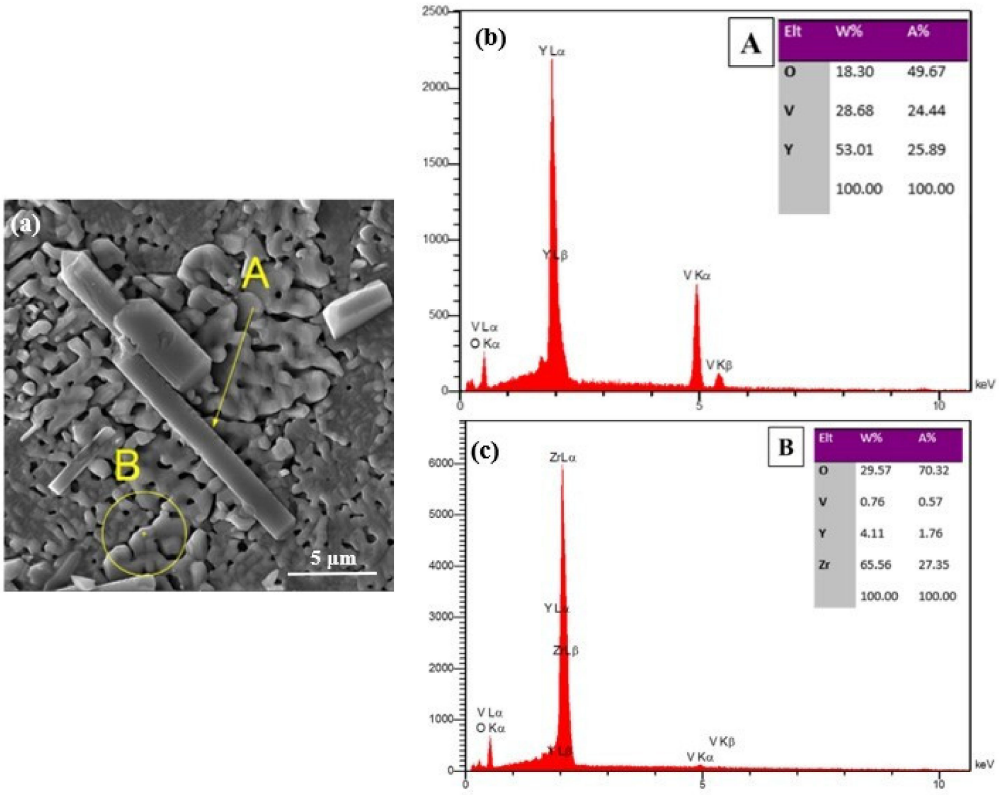

Figure 17. FE-SEM micrographs and EDS analysis of the direct laser sintering of EPD overlay after hot corrosion, (**a**) the surface of the coating, (**b**) EDS of point A, (**c**) EDS of area B.

The XRD patterns of plasma-sprayed YSZ coatings after 90 h of interaction at 1000 °C clearly reveal that a new phase formed, as shown in Figure 18a. Zirconia was found in both the nontransformable tetragonal (t′) phase and the monoclinic phase, as well as the presence of YVO_4 peaks. Part of the tetragonal ZrO_2 transformed into the monoclinic phase during the hot corrosion test. Hot corrosion is caused by interactions between the stabilizer phase of ZrO_2 and impurities such as sodium sulfate and vanadium pentoxide. As a result of the detrimental reactions, the stabilizer phase leaves the system, resulting in the change of tetragonal to monoclinic Zirconia, which causes TBC spallation [31,32]. The amounts of these phases were directly related to (i) exposure time, (ii) temperature, and (iii) surface state [33].

After laser treatment, the XRD pattern for the coatings revealed a Large amount of the t′ phase Figure 18b. Large amounts of the t′ phase were observed in the XRD pattern for the coatings after the laser treatment Figure 18b, indicating that the modified coating has significantly improved the phase stability in molten salt, which is desirable because the high phase stability is necessary for TBC applications. Obviously, the laser remelting coating had a lower fraction of monoclinic ZrO_2 as compared to plasma YSZ coating. The amounts of the harmful phase (m) were considerably reduced after the laser surface treatment. This reduction is due to the complete removal of void imperfections. The corrosion reactions of the molten salts with the surface of YSZ in the laser-treated layer were lower than in plasma-sprayed coatings due to the reduced specific surface area of the dense layer.

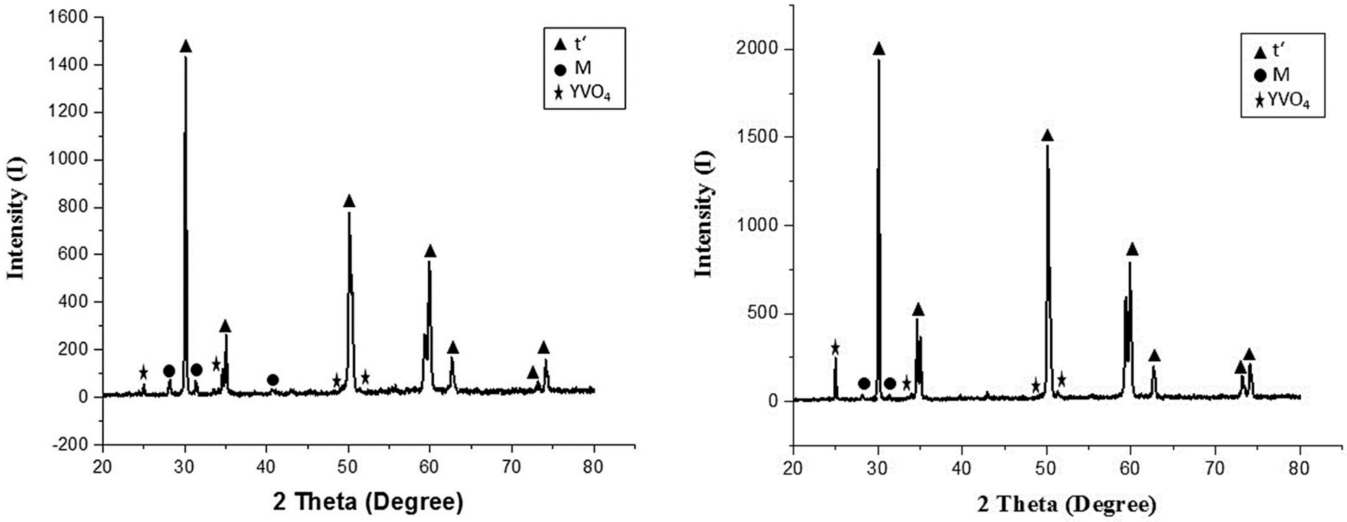

Figure 18. The XRD patterns of (**a**) plasma-sprayed and (**b**) direct laser sintering of EPD overlay after the hot corrosion test at 1000 °C for 90 h. using mixture salts of Na_2SO_4 + V_2O_5.

The linear least square approach was used to obtain the parabolic rate constants (Kp) (Hot corrosion rate constant) using the following equation:

$$(W/A)^2 = Kpt \quad (1)$$

where (W/A) is the weight gain per unit area (mg/cm^2), t is the exposure duration (hour), and Kp is the Parabolic rate constant (hot corrosion rate) ($mg^2\ cm^{-4}\ S^{-1}$).

The weight gain (mg/cm^2) for the samples subjected to hot corrosion was used to calculate the kinetics of hot corrosion. In comparison, plasma spraying coating resulted in a greater weight gain, whereas laser modification of the EPD overlay surface revealed lesser weight gain. As a result, the hot corrosion resistance in the molten salt environment was higher. The corrosion rate (Kp) value for the direct laser sintering of the EPD overlay was significantly lower than the plasma sprayed coating Table 6. This low corrosion rate (Kp) result also suggests that the laser surface modification of the coating layer is more resistant to the Na_2SO_4-55%V_2O_5 environment.

Table 6. The hot corrosion rate kp ($mg^2\ cm^{-4}\ s^{-1}$) measurements.

Specimens	Δw (g)	K_p ($mg^2\ cm^{-4}s^{-1}$)
Plasma sprayed coating	0.0025	2.3814×10^{-3}
Direct laser sintering of the EPD overlay	0.0013	6.4395×10^{-4}

4. Conclusions

(1) It is possible to utilize the EPD method to deposit a homogeneous, dense-continuous overlay coating of nano-YSZ onto a porous APS TBC surface as a protective layer;
(2) It is possible to sinter and modify the surface of the green EPD overlay in one step using laser treatment (direct laser sintering and modification);
(3) The direct laser sintering process can achieve promising results when implemented in one step, rather than carrying out two steps of sintering in a furnace and subsequent laser surface modification, thus shortening the application time while improving the performance;
(4) This technique can be used to produce a remelted overlay with a densified microstructure and a network of segmented cracks that are perpendicular to the surface of the TBCs underneath;

(5) The reliability of the microhardness value using Weibull's distribution was 1376 Hv after the laser sintering process of the YSZ EDP overlay, while the value without any improvement process was 603 Hv;
(6) The roughness reduction on the micro- and nanoscales was eightfold that of the plasma-sprayed coating. The value of the plasma-sprayed specimen was (8.609 μm, 4.38 nm), that of the EPD overlay was (5.36 μm, 2.32 nm), and that of the direct-laser-sintered specimen was (0.99 μm, 2.48 nm);
(7) The hot corrosion rate of the plasma sprayed coating was 2.3814×10^{-3} mg^2 cm^{-4} S^{-1}. This value decreased to 6.4395×10^{-4} mg^2 cm^{-4} S^{-1} after direct laser sintering of the EPD overlay.

Author Contributions: Conceptualization, M.A.A.B.; methodology, R.A.A.; writing—original draft preparation, M.A.A.B., R.A.A., S.A.A. and M.J.K.; writing—review and editing, M.A.A.B., R.A.A., S.A.A. and M.J.K.; supervision, M.A.A.B., S.A.A. and M.J.K. All authors have read and agreed to the published version of the manuscript.

Funding: This research received no external funding.

Institutional Review Board Statement: Not applicable.

Informed Consent Statement: Not applicable.

Data Availability Statement: Not applicable.

Conflicts of Interest: The authors declare no conflict of interest.

Appendix A

Table A1. The distribution of microhardness values following the direct laser sintering (DLS) of the YSZ EPD overlay. The value of 37% was obtained from Weibull's distribution.

No.	Microhardness (Hv)	Ln Hv	Si%	1/Si	ln(1/Si)	lnln(1/Si)	m	Hv at 37%Si
1	1809	7.500	5.263	19.000	2.944	1.079	5.144	≈1376
2	1724	7.452	10.526	9.500	2.251	0.811		
3	1715	7.447	15.789	6.333	1.845	0.612		
4	1689	7.431	21.052	4.75	1.558	0.443		
5	1576	7.362	26.315	3.800	1.335	0.288		
6	1560	7.352	31.578	3.166	1.152	0.142		
7	1378	7.228	36.842	2.714	0.998	−0.001		
8	1314	7.180	42.105	2.375	0.864	−0.145		
9	1308	7.176	47.368	2.111	0.747	−0.291		
10	1282	7.156	52.631	1.9	0.641	−0.443		
11	1226	7.111	57.894	1.727	0.546	−0.604		
12	1190	7.081	63.157	1.583	0.459	−0.777		
13	1131	7.030	68.421	1.461	0.379	−0.968		
14	1097	7.000	73.684	1.357	0.305	−1.186		
15	1088	6.992	78.947	1.266	0.236	−1.442		
16	1065	6.970	84.210	1.187	0.171	−1.761		
17	1030	6.937	89.473	1.117	0.111	−2.196		
18	957	6.863	94.736	1.055	0.054	−2.917		

References

1. Zhu, Q.; Chua, M.H.; Ong, P.J.; Lee, J.J.C.; Le Osmund Chin, K.; Wang, S.; Kai, D.; Ji, R.; Kong, J.; Dong, Z.; et al. Recent advances in nanotechnology-based functional coatings for the built environment. *Mater. Today Adv.* **2022**, *15*, 100270. [CrossRef]
2. El Gwad, S.A.A.; Morsi, M.S.; Ahmed, K.F. Characterization of Air Plasma Sprayed Al PO4 and LaserSealed ZrO_2-MgO Coatings on Ni-Base Supper Alloys of AeroEngine. *Int. J. Electrochem. Sci.* **2012**, *7*, 13020–13043. [CrossRef]
3. Ma, X.; Rivellini, K.; Ruggiero, P.; Wildridge, G. Novel Thermal Barrier Coatings with Phase Composite Structures for Extreme Environment Applications: Concept, Process, Evaluation and Performance. *Coatings* **2023**, *13*, 210. [CrossRef]
4. Kim, J.; Pyeon, J.; Kim, B.-G.; Khadaa, T.; Choi, H.; Zhe, L.; Dube, T.; Zhang, J.; Yang, B.-I.; Jung, Y.-G.; et al. Oxidation Behavior of NiCoCrAlY Coatings Deposited by Vacuum Plasma Spraying and High-Velocity Oxygen Fuel Processes. *Coatings* **2023**, *13*, 319. [CrossRef]
5. Tailor, S.; Mohanty, R.M.; Douba, A.V. Development of a new TBC system for more efficient gas turbine engine application. *Materials Today Proc.* **2016**, *3*, 2725–2734. [CrossRef]
6. Luo, L.; Chen, Y.; Zhou, M.; Shan, X.; Lu, J.; Zhao, X. Progress update on extending the durability of air plasma sprayed thermal barrier coatings. *Ceram. Int.* **2022**, *48*, 18021–18034. [CrossRef]
7. Courapied, D.; Kromer, R.; Berthe, L.; Peyre, P.; Costil, S.; Cormier, J.; Boustie, M.; Milhet, X. Laser adhesion test for thermal sprayed coatings on textured surface by laser. *J. Laser Appl.* **2016**, *28*, 022509. [CrossRef]
8. Jasim, A.N.; Abbass, M.K.; Jasim, M.; Salah, K. Synthesis, Characterization and Optimization of Electrophoretic Deposition (EPD) Parameters of YSZ Layer on Ti-6Al-4V Alloy substrate. *Mater. Sci. Eng.* **2020**, *745*, 012082. [CrossRef]
9. Abbas, R.A.; Ajeel, S.A.; Ali Bash, M.A.; Kadhim, M.J. The Influence of Spray Distance on the Assessment of Porosity in YSZ Thermal Barrier Coating. *AIP Conf. Proc.* **2022**, *2660*, 020096.
10. Rajasekaran, J.; Gnanasekaran, B.M.; Senthilkumar, T.; Kumaragurubaran, B.; Chandrasekar, M. Effect of thermal barrier coating for the improvement of si engine performance & emission characteristics. *Int. J. Res. Eng. Technol.* **2013**, *2*, 113–119.
11. Sanchez, I.; Axinte, D.; Liao, Z.; Gavalda-Diaz, O.; Smith, R. The effect of high strain rate impact in Yttria stabilized zirconia. *Mater. Des.* **2023**, *229*, 111908. [CrossRef]
12. Kulyk, V.; Duriagina, Z.; Kostryzhev, A.; Vasyliv, B.; Vavrukh, V.; Marenych, O. The Effect of Yttria Content on Microstructure, Strength, and Fracture Behavior of Yttria-Stabilized Zirconia. *Materials* **2022**, *15*, 5212. [CrossRef] [PubMed]
13. Abbas, R.A.; Ajeel, S.A.; Ali Bash, M.A.; Kadhim, M.J. Optimizing Coating Thickness of Electrophoretic Deposition Overlay on Plasma Sprayed YSZ Coating Using Taguchi Method. *IOP Earth Environ. Sci.* **2022**, *961*, 012060. [CrossRef]
14. Volpe, A.; Covella, S.; Gaudiuso, C.; Ancona, A. Improving the Laser Texture Strategy to Get Superhydrophobic Aluminum Alloy Surfaces. *Coatings* **2021**, *11*, 369. [CrossRef]
15. Omar, H.; Ibrahim, A.; Salem, H.; Sedky, S. Effect of Pulsed Laser on the Structure and Morphology of Alumina-Zirconia Coatings. *J. Surf. Eng. Mater. Adv. Technol.* **2013**, *3*, 249–256. [CrossRef]
16. Shankar, A.R.; Babu, B.J.; Sole, R.; Mudali, U.K.; Khatak, H.S. Laser remelting of plasma sprayed zirconia based ceramic coating for pyrochemical reprocessing applications. *Surf. Eng.* **2007**, *23*, 147–154. [CrossRef]
17. Jasim, K.M.; Atiyah, A.A.; Bash, M.A. In-situ laser pelletization of advanced ternary thermal barrier coating system. *Mater. Res. Express* **2019**, *6*, 035512. [CrossRef]
18. Reza, M.S.; Aqida, S.N.; Toff, M.R.M. An investigation of phase crystallinity in laser modified Yttria Stabilized Zirconia (YSZ) thermal barrier coating. *Key Eng. Mater.* **2014**, *611–612*, 1601–1607. [CrossRef]
19. Vafa, E.; Bazargan-Lari, R.; Bahrololoom, M.E. Electrophoretic deposition of polyvinyl alcohol/natural chitosan/bioactive glass composite coatings on 316L stainless steel for biomedical application. *Prog. Org. Coat.* **2021**, *151*, 106059. [CrossRef]
20. Parente, P.; Sanchez-Herencia, A.J.; Mesa-Galan, M.J.; Ferrari, B. Functionalizing Ti-Surfaces through the EPD of Hydroxyapatite/NanoY_2O_3. *J. Phys. Chem. B* **2013**, *117*, 1600–1607. [CrossRef]
21. Galvina, T.; Hyatt, N.C.; Rainforth, W.M.; Reaney, I.M.; Shepherd, D. Laser sintering of electrophoretically deposited (EPD) Ti_3SiC_2 MAX phase coatings on titanium. *Surf. Coat. Technol.* **2019**, *366*, 199–203. [CrossRef]
22. Baufeld, B.; van der Biest, O.; Ratzer-Scheibe, H.-J. Lowering the sintering temperature for EPD coatings by applying reaction bonding. *J. Eur. Ceram. Soc.* **2008**, *28*, 1793–1799. [CrossRef]
23. Antou, G.; Montavon, G.; Françoise, H.; Cornet, A.; Coddet, C.; Machi, F. Modification of thermal barrier coating architecture by in situ laser remelting. *J. Eur. Ceram. Soc.* **2006**, *26*, 3583–3597. [CrossRef]
24. Wang, W.; Qian, S.Q.; Shen, H. Microstructure and Mechanical Properties of Yttria-Stabilized Zirconia Coatings Produced by Eletrophoretic Deposition and Microwave Sintering. *Metall. Mater. Trans. A* **2011**, *42*, 3265–3268. [CrossRef]
25. Desiati, R.D.; Anawati, A.; Sugiarti, E. Two-Step Sintering Improved Compaction of Electrophoretic-Deposited YSZ Coatings. *J. Mater. Eng. Perform.* **2022**, *31*, 9888–9899. [CrossRef]
26. Antonelli, E.; Andreeta, M.R.B.; Botero, E.R.; Hernandes, A.C. Thick Film Laser Sintering: An Evidence for Two-step Process. *Open Crystallogr. J.* **2013**, *6*, 1–6. [CrossRef]
27. Wang, Y.; Liu, J.; Liao, H.; Darut, G.; Stella, J.; Poirier, T.; Planche, M.-P. Influence of Laser Glazing on the Characterization of Plasma-Sprayed YSZ Coatings. *J. Therm. Spray Technol.* **2017**, *26*, 93–99. [CrossRef]
28. Ahmadi-Pidanin, R.; Shoja-Razavi, R.; Mozafarinia, R.; Jamalin, H. Laser surface modification of plasma sprayed CYSZ thermal barrier coatings. *Ceram. Int.* **2013**, *39*, 2473–2480. [CrossRef]

29. Jasim, K.M.; Rawlings, R.D.; West, D.R.F. Pulsed laser sealing of plasma-sprayed layers of 8 wt % yttria-stabilized zirconia. *J. Mater. Sci.* **1992**, *27*, 3903–3910. [CrossRef]
30. Abbas, R.A.; Ajeel, S.A.; Ali Bash, M.A.; Kadhim, M.J. Effect of plasma spray distance on the features and hardness reliability of YSZ thermal barrier coating. *Mater. Today: Proc.* **2021**, *42*, 2553–2560. [CrossRef]
31. Zhang, P.; Zhang, X.; Li, F.; Zhang, Z.; Li, H.; Wang, Y.; Ren, L.; Liu, M. Effects of Selective Laser Modification and Al Deposition on the Hot Corrosion Resistance of Ceria and Yttria-Stabilized Zirconia Thermal Barrier Coatings. *Coatings* **2019**, *9*, 353. [CrossRef]
32. Zhang, P.; Zhang, X.; Li, F.; Zhang, Z.; Wang, Y.; Li, H.; Ren, L.; Liu, M. Hot Corrosion Behavior of YSZ Thermal Barrier Coatings Modified by Laser Remelting and Al Deposition. *J. Therm. Spray Tech.* **2019**, *28*, 1225–1238. [CrossRef]
33. Zhou, P.; Wang, Y.; Liu, Q.; Qiao, Y.; Chen, S. Hot Corrosion Behavior of Co–Al–W Superalloys with Si Additions. *Coatings* **2023**, *13*, 1031. [CrossRef]